Variability of the net air-sea CO2 flux inferred from shipboard and satellite measurements in the Southern Ocean south of Tasmania and New Zealand

Yvan Rangama, Jacqueline Boutin, Jacqueline Etcheto, Liliane Merlivat, Taro Takahashi, Bruno Delille, M. Frankignoulle, Dorothee C. E. Bakker

Variability of the net air–sea CO_2 flux inferred from shipboard and satellite measurements in the Southern Ocean south of Tasmania and New Zealand

Y. Rangama,[1] J. Boutin,[1] J. Etcheto,[1] L. Merlivat,[1] T. Takahashi,[2] B. Delille,[3] M. Frankignoulle,[3,4] and D. C. E. Bakker[5]

Received 23 July 2004; revised 27 March 2005; accepted 18 May 2005; published 8 September 2005.

[1] We determine the distribution of oceanic CO_2 partial pressure (pCO_2) with respect to remotely sensed parameters (sea surface temperature (SST) and chlorophyll (Chl)) in order to gain an understanding of the small-scale (10–100 km) pCO_2 variability and to estimate the net air–sea CO_2 flux in the region (125°E–205°E; 45°S–60°S), which represents 22% of the Southern Ocean area between 45°S and 60°S. We split the study area into several biogeochemical provinces. In chlorophyll-poor regions, pCO_2 is negatively correlated with SST, indicating that pCO_2 is mostly controlled by mixing processes. For Chl > 0.37 mg m^{-3}, pCO_2 is negatively correlated with Chl, indicating that pCO_2 variability is mostly controlled by carbon fixation by biological activity. We deduce fields of pCO_2 and of air–sea CO_2 fluxes from satellite parameters using pCO_2-SST, pCO_2-chlorophyll relationships and air–sea gas exchange coefficient, K, from satellite wind speed. We estimate an oceanic CO_2 sink from December 1997 to December 1998 of -0.08 GtC yr^{-1} with an error of 0.03 GtC yr^{-1}. This sink is approximately 38% smaller than that computed from the Takahashi et al. (2002) climatological distribution of ΔpCO_2 for the 1995 year but with the same K (-0.13 GtC yr^{-1}). When we correct ocean pCO_2 for the interannual variability between 1995 and 1998, the difference is even larger, and we cannot reconcile both estimates in February–March and from June to November. This strengthens the need of new in situ measurements for validating extrapolation methods and for improving knowledge of interannual pCO_2 variability.

Citation: Rangama, Y., J. Boutin, J. Etcheto, L. Merlivat, T. Takahashi, B. Delille, M. Frankignoulle, and D. C. E. Bakker (2005), Variability of the net air–sea CO_2 flux inferred from shipboard and satellite measurements in the Southern Ocean south of Tasmania and New Zealand, *J. Geophys. Res.*, *110*, C09005, doi:10.1029/2004JC002619.

1. Introduction

[2] In situ measurements of sea surface CO_2 partial pressure indicate that the Southern Ocean may be a large oceanic sink for atmospheric CO_2. Actually, the climatological net air–sea flux of CO_2 reconstructed from such measurements by *Takahashi et al.* [2002] shows strong sinks between 40°S and 60°S; compiling measurements from several campaigns in the subantarctic zone (SAZ) of the Southern Ocean, *Metzl et al.* [1999] estimated that the absorbed flux of CO_2 might be up to 1 GtC yr^{-1} in the whole SAZ. However, the air–sea CO_2 fluxes estimated in the Southern Ocean using atmospheric inversions [*Gurney et al.*, 2004], ocean biogeochemical models and oceanic inversions [*Gloor et al.*, 2003] are smaller than that deduced from in situ measurements. Recently, *Gloor et al.* [2003] estimated an uptake of -0.3 GtC yr^{-1} between 36°S and 58°S in the Indian and Pacific sectors of the Southern Ocean using an inverse oceanic model. The fluxes for the same region were estimated as -0.4 GtC yr^{-1} from atmospheric transport models, while the CO_2 sink in the Takahashi climatology is close to -0.8 GtC yr^{-1}.

[3] The air–sea CO_2 flux is classically estimated from ocean-surface measurements as the product of the local air–sea CO_2 exchange coefficient (K) and partial pressure difference (ΔpCO_2). The regional flux is derived by the integration of the local flux over a given region. The main unknown when dealing with the spatial distribution and the temporal variability of the air–sea flux comes from the ΔpCO_2 variability which is poorly known, due to the complex physical and biogeochemical processes governing the sea surface partial pressure (pCO_2) and to the scarcity of in situ measurements in these remote and rough waters. Although the absolute value of K is not well fixed, its spatial and temporal variability is relatively well known as

[1]Laboratoire d'Océanographie Dynamique et de Climatologie/Institut Pierre Simon Laplace, Université Pierre et Marie Curie, Paris, France.
[2]Lamont-Doherty Earth Observatory of Columbia University, Palisades, New York, USA.
[3]Unité d'Océanographie Chimique, MARE, Université de Liège, Liège, Belgium.
[4]Deceased 13 March 2005.
[5]School of Environmental Sciences, University of East Anglia, Norwich, UK.

0148-0227/05/2004JC002619

Table 1. List of Shipboard Campaigns

Cruise Area	Cruise Name	Start Cruise	End Cruise	Season	Ship Name
East of New Zealand	NBP 97 8	06/11/1997	11/11/1997	spring	R/V *Nathaniel B. Palmer*
(AESOPS campaigns)	RR KIWI 8 first transect	08/01/1998	13/01/1998	summer	R/V *Roger A. Revelle*
	RR KIWI 8 second transect	03/02/1998	07/02/1998	summer	
	RR KIWI 9 first transect	13/02/1998	26/02/1998	summer	
	RR KIWI 9 second transect	07/03/1998	18/03/1998	fall	
	NBP 98 2	25/03/1998	02/04/1998	fall	R/V *Nathaniel B. Palmer*
South of Tasmania	dta 99	22/10/1999	28/10/1999	spring	R/V *Astrolabe*
(Astrolabe campaigns)	rta 99	21/12/1999	26/12/1999	summer	
South of New Zealand and Tasmania	first SOIREE transect	02/02/1999	09/02/1999	summer	R/V *Tangaroa*
(SOIREE campaigns)	second SOIREE transect	22/02/1999	28/02/1999	summer	

a result of the good coverage of satellite wind speed measurements.

[4] Main processes controlling the variability of pCO_2 are oceanic circulation, thermodynamical effects, biological carbon uptake and air–sea gas exchange. Schematically, oceanic circulation promotes pCO_2 variations by mixing and transport of water masses with different properties (dissolved inorganic carbon, temperature, salinity, etc.); the thermodynamical effect is caused by the dependence of the CO_2 solubility and dissociation constants on temperature; biological activity is responsible for carbon fixation and release.

[5] The objective of our paper is to determine the spatial distribution of the air–sea CO_2 flux and its seasonal variation over a region of the Southern Ocean south of Tasmania and New Zealand.

[6] Our study was limited to 1.5 years in order to minimize uncertainties from possible interannual variations in surface ocean pCO_2. Specifically, the effect of the increase of the atmospheric CO_2 concentration on pCO_2 in the Southern Ocean is poorly known and it may reach 3 μatm over 2 years. Therefore we choose to limit our study to less than 2 years and to a region for which both satellite chlorophyll and in-situ campaigns in several seasons are available. This study focuses on the area south of Tasmania and New Zealand (125°E–205°E; 45°S–60°S) from December 1997 to December 1998, where several shipboard campaigns were carried out at a time when the Advanced Very High Resolution Radiometer (AVHRR) and the Sea-viewing Wide-Field-of view Sensor (SeaWiFS) satellites were making measurements of sea surface temperature (SST) and of ocean color, respectively.

[7] In section 2, we present the data; in section 3, we analyze observed pCO_2 variability and in section 4 we describe pCO_2 extrapolation and associated errors. In section 5, we present air–sea fluxes and comparison with the *Takahashi et al.* [2002] climatological mean estimates. The results are discussed in section 6.

2. Data

2.1. In Situ pCO_2

[8] We study oceanic pCO_2 measurements made in the area south of Tasmania and southeast of New Zealand during various campaigns. We only use data after September 1997 when the chlorophyll content extracted from SeaWiFS chlorophyll images is available: two Astrolabe campaigns conducted in the course of opportunistic logistical cruises by the University of Liege during spring and summer south of Tasmania and four Antarctic Environment and Southern Ocean Process Study (AESOPS) campaigns conducted during spring, summer, and fall south east of New Zealand (P.I: T. Takahashi) (see Table 1 for more details and Figure 1a for the location of the transects). In addition, data collected during two Southern Ocean Iron Release Experiment (SOIREE) transects are used to validate the extrapolation method. Even though we use AESOPS campaigns conducted during a restricted period, it can be seen in the work of *Morrison et al.* [2001] that these data are consistent with those from other years at the southern edge of the studied area; it is also true at lower latitudes. Hence we consider that our analysis is based on a representative year.

[9] We eliminate data collected over the continental shelves (water depth less than 500m), using the same criteria as *Moore and Abbott* [2000], retaining only pCO_2 measurements made in the open ocean. This correction is applied to three AESOPS transects (NBP 97 8, RR KIWI 9, and NBP 98 2), which cross the Bounty plateau at about 180°E, 48°S.

2.1.1. Astrolabe Campaigns

[10] A complete description of the experimental set-up is given by *Frankignoulle et al.* [2001]. xCO_2 accuracy is estimated to be 2ppm, the precision on the order of ±0.5 ppm. The estimation of pCO_2 from CO_2 concentration measurements is described in Appendix A. Given uncertainties linked to the atmospheric pressure correction, we estimate pCO_2 precision to be about ±2 μatm.

2.1.2. AESOPS Campaigns

[11] The method for measuring pCO_2 in surface water during the AESOPS campaigns is described by *Takahashi et al.* [2000]; the overall pCO_2 precision is estimated to be ±1.5 μatm. We use data available on http://www1.whoi.edu/southern.html that are shown in the work of *Rubin* [2003]. We do not use the pCO_2 measurements collected during the RR KIWI 8 campaign (first leg from 8 January 1998 to 13 January 1998) between 49°S and 45°S, since there are wide gaps in the data.

2.1.3. SOIREE Campaigns

[12] We use pCO_2 measured during two SOIREE transects conducted during February 1999 south of Australia. Figure 2 shows the location of these transects superimposed on the monthly SeaWiFS chlorophyll distribution for February 1999 south of Australia. The transects cross the center of the study area, between 142°E and 170°E, a region not explored by AESOPS and Astrolabe campaigns, thus allowing us to check the ability of our regression method to reproduce pCO_2 at different locations. The method of the

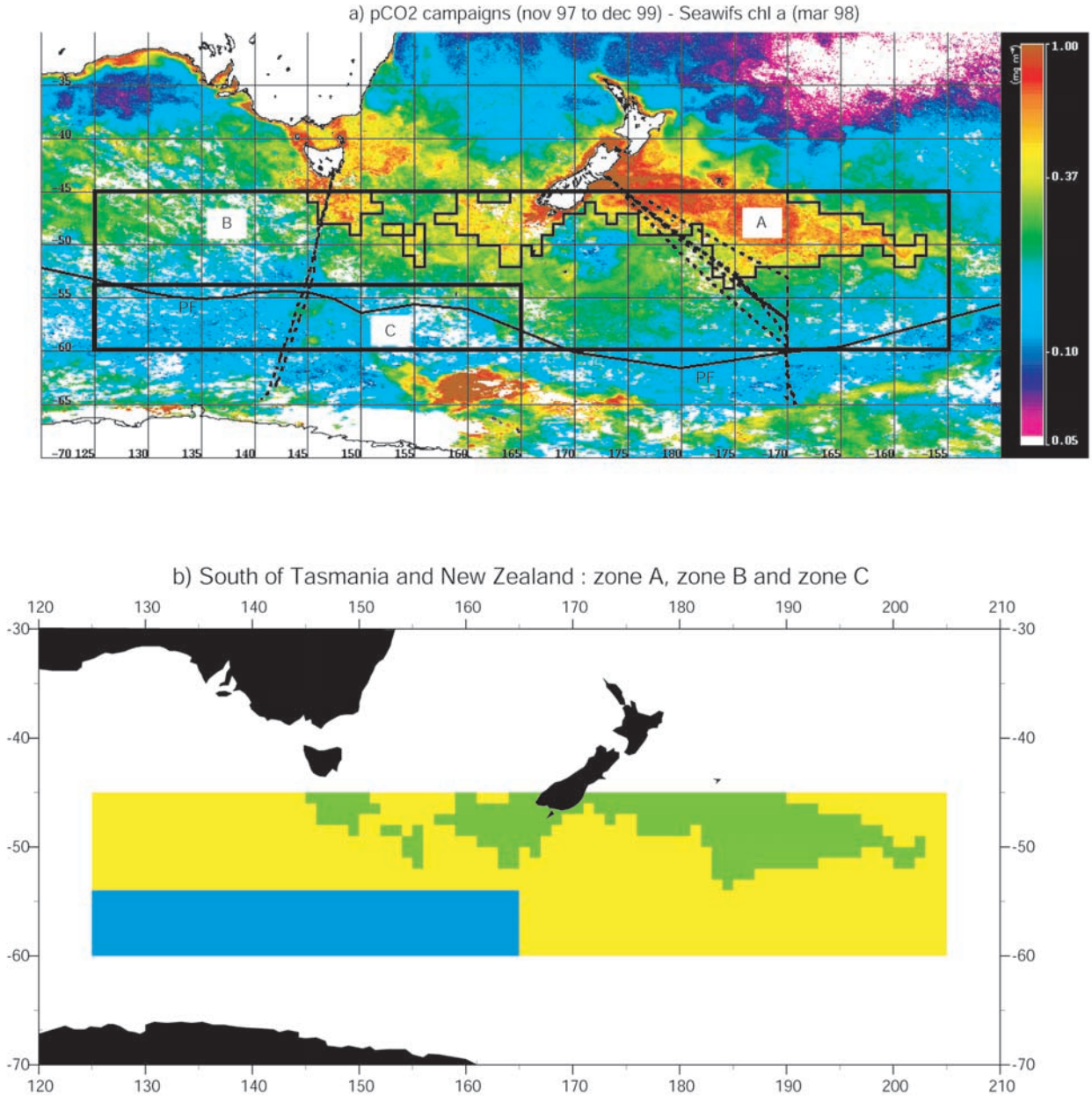

Figure 1. (a) Tracks of the campaigns (dashed lines; AESOPS campaigns in the eastern part, Astrolabe campaigns in the western part) superimposed on a SeaWiFS chlorophyll map (March 1998). The climatological Polar Front (PF) from *Belkin and Gordon* [1996] and the boundaries between zones A, B, and C are indicated in solid lines. (b) Zone A (chlorophyll-rich region; green), B (yellow), and C (blue) for March 1998.

surface water pCO_2 measurements is described by *Watson et al.* [2000] and by *Bakker et al.* [2001]. The accuracy and precision of the measurements are estimated to be 1.0 and 0.6 μatm, respectively.

2.2. Satellite Parameters

[13] We use SST derived by the National Meteorological Center (NMC) from in situ and AVHRR data using the *Reynolds and Smith* [1994] objective interpolation analysis and level 3 SeaWiFS chlorophyll data (version 3) distributed by the Physical Oceanography Distributed Active Archive Center (PODAAC). Reynolds SST data grids have a 1 × 1 degree resolution and SeaWiFS chlorophyll (Chl) data grids have a 9 × 9 km resolution. We use weekly 9 km SeaWIFS Chl to develop the extrapolation scheme. Monthly grids of SST and Chl are used to extrapolate pCO_2.

[14] We use level 2 ERS-2 wind products (instantaneous; 25 km resolution) delivered by the Institut Français de Recherche pour l'Exploitation de la Mer (IFREMER)/ Centre ERS d'Archivage et de Traitement (CERSAT) in Brest, France, to derive the gas exchange coefficient, K. K is derived from Reynolds SST, ERS-2 satellite wind speed (U) data and a K–U relationship. The air–sea flux differences induced by the use of different K-U parameterizations were already documented by *Boutin et al.* [2002]. We do

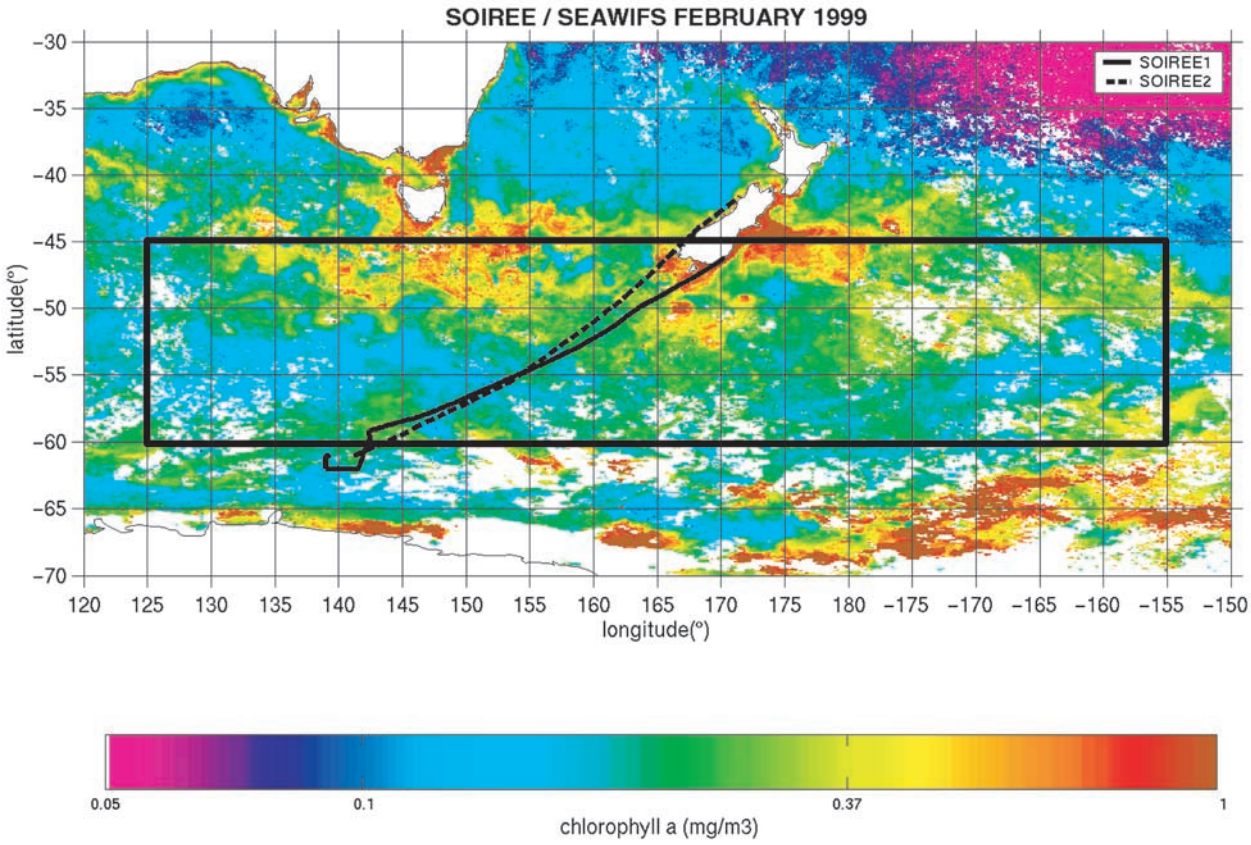

Figure 2. SOIREE transects superimposed on the SeaWiFS chlorophyll map for February 1999.

not consider here a cubic relationship, as proposed by *Wanninkhof and McGillis* [1999] as the cubic dependency has not been firmly confirmed on recent experiments: analysis of measurements in the Southern Ocean by [*Wanninkhof et al.*, 2004] does not allow to distinguish between a cubic and a quadratic relationship; *Frew et al.* [2004] found that the best fit to the CoOP97 measurements follow a quadratic K-U relationship close to the [*Nightingale et al.*, 2000] relationship. In our study area, K derived from the *Liss and Merlivat* [1986] and *Nightingale et al.* [2000] parameterizations are systematically lower than the one deduced from the *Wanninkhof* [1992] U^2 formulation by a factor 1.8 and 1.2 respectively (Figure 3). Whatever the relationship is used, K varies seasonnaly by a factor 1.4 between winter and summer. In the following we will use the *Wanninkhof* [1992, relation 3] K–U relationship for short-term wind speed as it is the most widely used in the literature; using other K-U parameterization would lead to different absolute values of air–sea CO_2 flux as discussed by *Boutin et al.* [2002], but the relative differences between fluxes deduced from various Δp fields would remain in the same proportions as K shown in Figure 3. In particular, according to recent studies by *Peacock* [2004] and *Sweeney et al.* [2004], ^{14}C inventory used to calibrate *Wanninkhof* [1992] relationship could be overestimated by 15 to 25% so that absolute values of our flux estimates could be overestimated as well. To take into account small-scale variability of wind speed, K values are computed for each ERS-2 measurement (instantaneous, 25 km resolution). Then, K

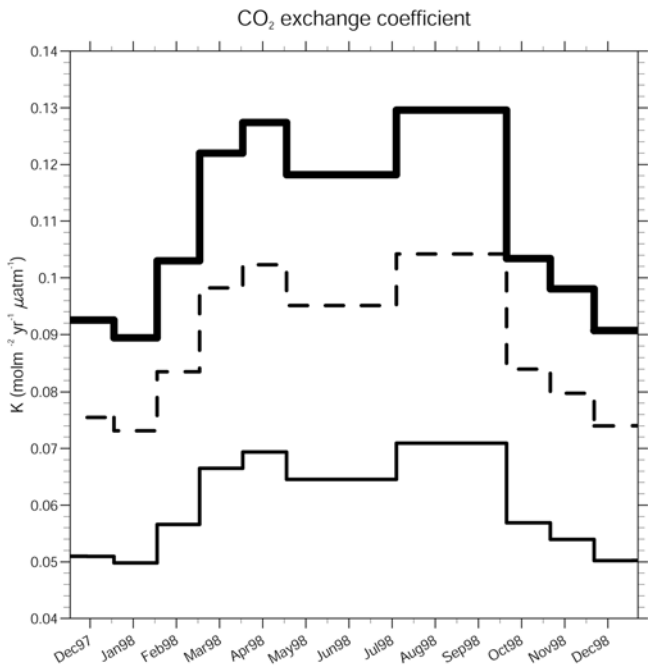

Figure 3. CO_2 exchange coefficient averaged over the study area and derived from *Wanninkhof* [1992] relationship (thick line), *Nightingale et al.* [2000] relationship (dashed line) and *Liss and Merlivat* [1986] relationship (thin line) for the year 1998.

Table 2. Summary of the Relations[a]

Zones	Seasons or Months	Fits or $\langle pCO_2 \rangle$ *Chl* in mg.m^{-3}, *SST* in °C and pCO_2 in μatm	Std[e] in μatm	Stdfit[e] in μatm	Number of Data
Zone A: chl-"rich" area	spring, summer, fall and winter[b]	$pCO_2 = -33.04 \times Chl. + 347.89$	11.3	7.9	209
chl-"rich" area in the southwestern area (region C)	December and January only	$pCO_2 = -33.04 \times Chl. + 363.$	...	...	...
Zone B: chl-"poor" area	spring	$pCO_2 = -2.69 \times SST + 370.80$	8.2	5.7	1155
	summer December	$pCO_2 = -1.23 \times SST + 352.50$	5.8	4.8	368
	summer January	$pCO_2 = \langle pCO_2 \rangle = 334$	9.3	...	1205
	summer February	$pCO_2 = \langle pCO_2 \rangle = 348$	9.2	...	3083
	fall	$pCO_2 = -2.06 \times SST + 362.63$	4.2	2.6	3042
	winter	$pCO_2 = -2.38 \times SST + 366.72$[c]	...	...	...
Zone C: southwestern area	spring	$pCO_2 = \langle pCO_2 \rangle = 357$	4.0	...	365
	summer	$pCO_2 = \langle pCO_2 \rangle = 357$	6.5	...	298
	fall	$pCO_2 = \langle pCO_2 \rangle = 350$	2.3	...	1167
	winter	$pCO_2 = \langle pCO_2 \rangle = 354$[d]	...	...	...

[a]Used to extrapolate pCO_2 and statistics of the residuals to the fits.
[b]No winter data: the same fit is used for winter.
[c]The pCO_2–SST fit in spring and in fall are averaged to compute this new linear fit.
[d]Here $pCO_2 = \frac{\langle pCO_2 \rangle in\ spring + \langle pCO_2 \rangle in\ fall)}{2}$.
[e]Here stdfit, standard deviation of pCO_2 with respect to the fits; std, standard deviation of pCO_2 measurements.

values are interpolated over a 1 × 1 degree grid using an objective analysis described by *Boutin et al*. [1995].

2.3. Atmospheric pCO_2

[15] In order to deduce maps of ΔpCO_2 from maps of extrapolated pCO_2, we use atmospheric concentration of CO_2 in dry air (atmospheric xCO_2) provided by *Globalview–CO_2* [2003, available via anonymous FTP at ftp.cmdl.noaa.gov, path: ccg/co2/GLOBALVIEW] at Cape Grim station in Tasmania (144.68°E; 40.68°S) and we assume that this value is equal to the atmospheric xCO_2 mean value over the area (125°E–205°E; 60°S–45°S). We estimate monthly maps of atmospheric pCO_2, pCO_{2a}, at 1° × 1° resolution using equation (A1), monthly atmospheric xCO_2, ECMWF maps of atmospheric pressure, Patm, and saturated water pressure, pH_2O. pH_2O is computed from Reynolds SST grids (monthly, 1 × 1 degree resolution) using the formulation of *Weiss and Price* [1980]. ECMWF Patm maps represent the field at sea level, originally at 2.5° × 2.5° resolution that we subsampled to 1° × 1° resolution.

3. Correlation of Oceanic pCO_2 With Chlorophyll and SST

[16] First, we look for biogeochemical provinces inside which in situ pCO_2 measurements appear to have a similar behavior with respect to SST and chlorophyll. Next, inside each zone, we look for a relationship between pCO_2 and SST or chlorophyll. The pCO_2–SST relationships take into account pCO_2 variability induced by mixing and thermodynamic effects. In addition, the use of chlorophyll data enables the biological effect to be taken into account.

[17] We use different combinations of in situ data (campaign by campaign, seasonal, annual, etc.) in various regions. pCO_2 is expected to have a seasonal variation but this could not be shown from the measurements themselves because of large spatial variations. We decide to arbitrarily split the measurements by seasons as defined by *Moore and Abbott* [2000]: summer (December to February), fall (March to May), winter (June to August), and spring (September to November).

[18] Given the large scatter of data we only test linear fits between pCO_2 and SST and between pCO_2 and chlorophyll. We do not use multiparametric fits between pCO_2-SST-Chl because in such fits, the variability of pCO_2 is split in two parts, one coming from SST variability and one coming from the chlorophyll variability. Therefore this division of pCO_2 variability is quite artificial because SST and Chl are correlated; on the other hand, the residuals of the pCO_2-Chl fits are not correlated with SST (see below).

[19] We analyze the quality of the fits using the standard deviation of the difference between measured pCO_2 and pCO_2 predicted by the fit, stdfit. When stdfit is not significantly smaller than the standard deviation of pCO_2 measurements, std, our fit does not improve the pCO_2 prediction compared to taking a constant value for pCO_2. In that case or in case the correlation coefficient is less than 0.5, we take a constant pCO_2 value.

3.1. The pCO_2 Variability Correlated With Chlorophyll

[20] To get pCO_2 at a resolution close to that of SeaWiFS level 3 data (9 × 9 km), we average pCO_2 for areas 0.08° in latitude and in longitude, hereafter called pCO_2(9 km). Then, we collocate pCO_2(9km) measurements with weekly 9 km SeaWiFS chlorophyll maps. The weekly SeaWiFS data are chosen as a compromise between minimizing data gaps due to cloud coverage (very frequent on daily images) and maintaining the temporal evolution of the chlorophyll content inside one month (we observe significant temporal changes from one week to the next).

[21] We always find a chlorophyll-rich zone in the northern part of each transect. Its mean southern limit is 49°S and 48°S on the eastern and western campaigns, respectively. When comparing collocated chlorophyll and pCO_2 measurements campaign by campaign, we observe a negative correlation between the two parameters in the chlorophyll-rich zone. We empirically derive a chlorophyll threshold equal to 0.37 mg m^{-3} to define the chlorophyll-rich zone in which such a correlation is observed. This limit is adopted because the accuracy of the chlorophyll content retrieved from SeaWiFS measurements decreases for low

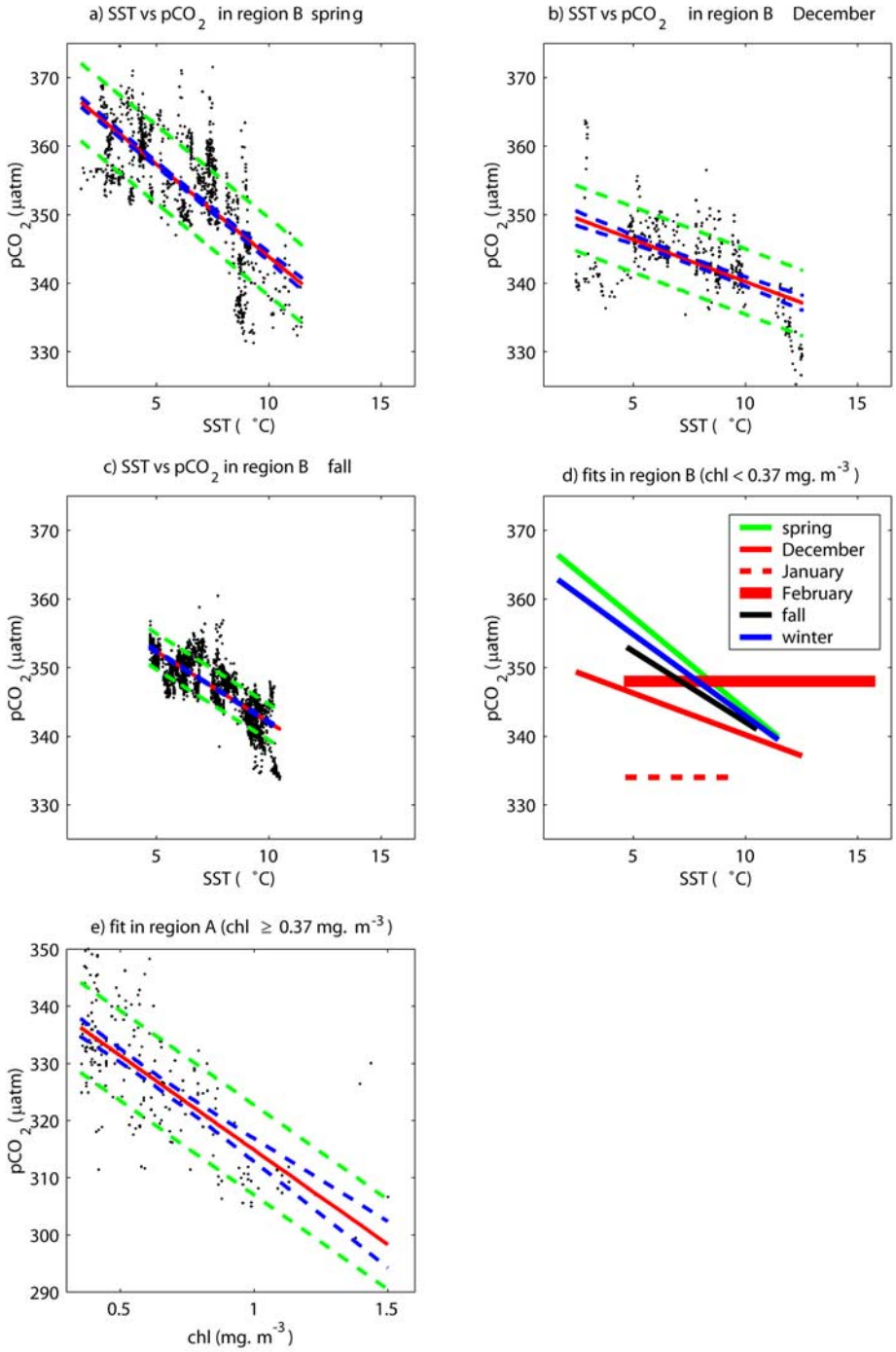

Figure 4. Linear fit (red), its 95% confidence interval (blue dashed line), and the pCO_2 residuals with respect to the fits (±stdfit) (green dashed line) superimposed on the pCO_2–SST scatterplot for zone B in (a) spring, (b) December and (c) fall; (d) Summary of pCO_2–SST relationships used in the paper (including mean values) plotted over the SST ranges covered by the measurements. (e) Same as (a) for a yearly pCO_2–chlorophyll fit in zone A (for chl $\geq$ 0.37 mg m^{-3}).

values, thus hampering the comparison in chlorophyll-poor regions. The chlorophyll-rich zone will be referred to as zone A from here on. Its limit is found from monthly 1 × 1 degree SeaWiFS images rather than from weekly 9 × 9 km images, in order to avoid data gaps due to cloud coverage, and this varies from month to month with changes in chlorophyll. An example is given in Figures 1a and 1b for March 1998. Zone A includes a southern part of the subtropical frontal zone (not shown in Figure 1a) and a northern part of the subantarctic zone.

[22] The best pCO_2–chlorophyll fit in zone A is obtained when all data for spring, summer and fall are pooled; it is

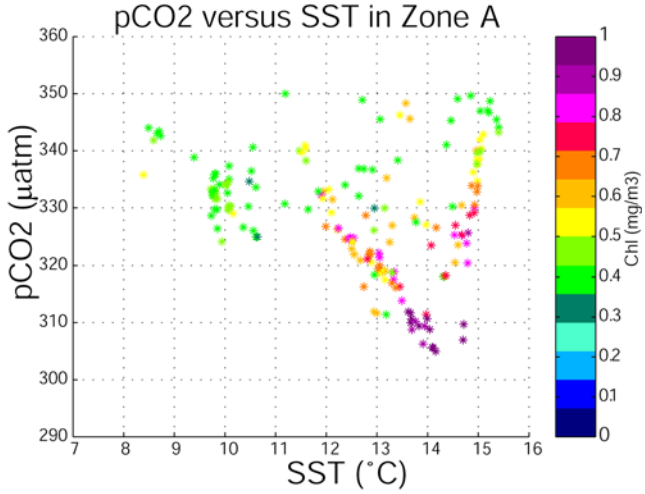

Figure 5. The pCO_2 versus SST for AESOPS and Astrolabe campaigns in Zone A; Chl is color coded. High chlorophyll values corresponding to low pCO_2 values are only observed at high SST. Nevertheless, pCO_2-SST fit is of lower quality than pCO_2-Chl fit.

indicated in Table 2 and Figure 4e. High chlorophyll are only observed for high SST so that chlorophyll and SST appears to be correlated (r = 0.65); low pCO_2 also appears for high SST (Figure 5), but the corresponding pCO_2-SST fit is of poorer quality (stdfit = 8.6 µatm) and not used in the following. In addition, the residuals of pCO_2-Chl fits are not correlated with SST (r = 0.1).

3.2. The pCO_2 Variability Correlated With SST

[23] In the rest of the study area (Chl < 0.37mg m^{-3}), we find a sharp latitudinal SST and pCO_2 gradient at about 54°S on the Astrolabe measurements corresponding to the position of the Polar Front (PF) (see Figure 1a). We divide the remaining area into two zones; schematically zone B north of the Polar Front and zone C south of the Polar Front (see Figure 1a). We do not find any clear latitudinal pCO_2 and SST gradient corresponding to the climatological Subantarctic Front (SAF) derived either from *Orsi et al.* [1995] or from *Belkin and Gordon* [1996] (not shown in Figure 1a). Hence we keep data from the SAZ and from the polar zone together.

[24] For zone B, in spring and fall, we establish seasonal negative correlations between pCO_2 and SST (see Table 2 and Figure 4a, 4c, and 4d). These fits are similar, but their 95% confidence intervals do not overlap indicating that they are statistically different. In addition, we test a pCO_2–SST fit from spring and fall data together: in that case, stdfit is much larger (4.1 µatm) than stdfit for fall data only (2.6 µatm), so we decide to keep one fit for each season. In summer, we find a significant negative correlation only for December. For January and February, the pCO_2–SST correlation coefficient is less than 0.5, so we do not take into account the pCO_2 changes due to the SST variations but use an average pCO_2 value. Since no measurement is available for winter, a winter pCO_2–SST relationship is derived by averaging the coefficients of the pCO_2–SST fit for spring and fall.

[25] In zone C, we do not find any correlation between pCO_2 and SST; consequently we use the seasonal pCO_2 average derived from the Astrolabe measurements in spring and summer. In fall, since we have no data for zone C, we take the average of the AESOPS pCO_2 measurements in the same latitude range. In winter, pCO_2 is assumed to be equal to the average of the spring and fall values.

3.3. Interpretation of Observed pCO_2 Relationships With Chl and SST

[26] Finding a pCO_2–chlorophyll or a pCO_2–SST fit does not mean that only biological or physical mechanisms are at work, but rather that a particular mechanism dominates the small-scale (10–100 km) variability. In fact, a biological contribution may be included in an SST fit since the biological activity tends to be higher in warm water. A physical contribution may be included in a chlorophyll fit as well since mixing affects biology.

[27] We find that the ocean is undersaturated in most of the study area, implying that biology is decreasing the average pCO_2 even in zone B. However, in this zone, we could not show any short-scale pCO_2–chlorophyll correlation. There are several reasons for this absence of correlation: biological export involves slow and weakly variable mechanisms that may be hiden by more variable processes; a strong carbon fixation may have occurred outside of our study area and the waters with reduced CO_2 may have been advected in zone B; subsurface chlorophyll may be different from the surface chlorophyll visible from space. However, a quantitative study of the processes responsible for this undersaturation would require more data in order to describe the historic of water masses. Conversely in zone A where chlorophyll gives the best fit, it means that the thermodynamical and mixing effects more or less compensate each other, at small-scale, leaving a dominant short-term biological signature.

[28] This coupling between physical and biological effects is illustrated by the test described below. Instead of comparing pCO_2 at measured SST to chlorophyll, we used pCO_2 at constant temperature, correcting for the thermodynamical effect using the formulation of *Takahashi et al.* [2002, relation 1] (isochemical conditions are assumed here):

$$(pCO_2 \text{ at } T_{cst}) = (pCO_2)_{obs} . \exp[0.0423(T_{cst} - T_{obs})] \quad (1)$$

where T is the sea surface temperature in °C and the subscript "cst" and "obs" indicate constant and observed values, respectively. Here pCO_2 at constant temperature is taken as a proxy for the total carbon content.

[29] In all cases, the correlation coefficient is higher when using pCO_2 normalized at constant temperature. However, this does not mean that the fit of (pCO_2 at T_{cst}) is better suited for the simulation of (pCO_2 at T_{obs}) than the fit obtained from pCO_2 at T_{obs}. Actually, the correlation coefficient is defined as $r = \sqrt{1 - (stdfit^2/std^2)}$ and stdfit for the fit of (pCO_2 at T_{cst}) and for the fit of (pCO_2 at T_{obs}) are similar while std of (pCO_2 at T_{cst}) is much larger than std of (pCO_2 at T_{obs}) (more than 30 and 10 µatm respectively). In fact, when (pCO_2 at T_{cst}) regressions are used to predict pCO_2 at measured SST using the inverse of equation (1), the standard deviation of the predicted minus

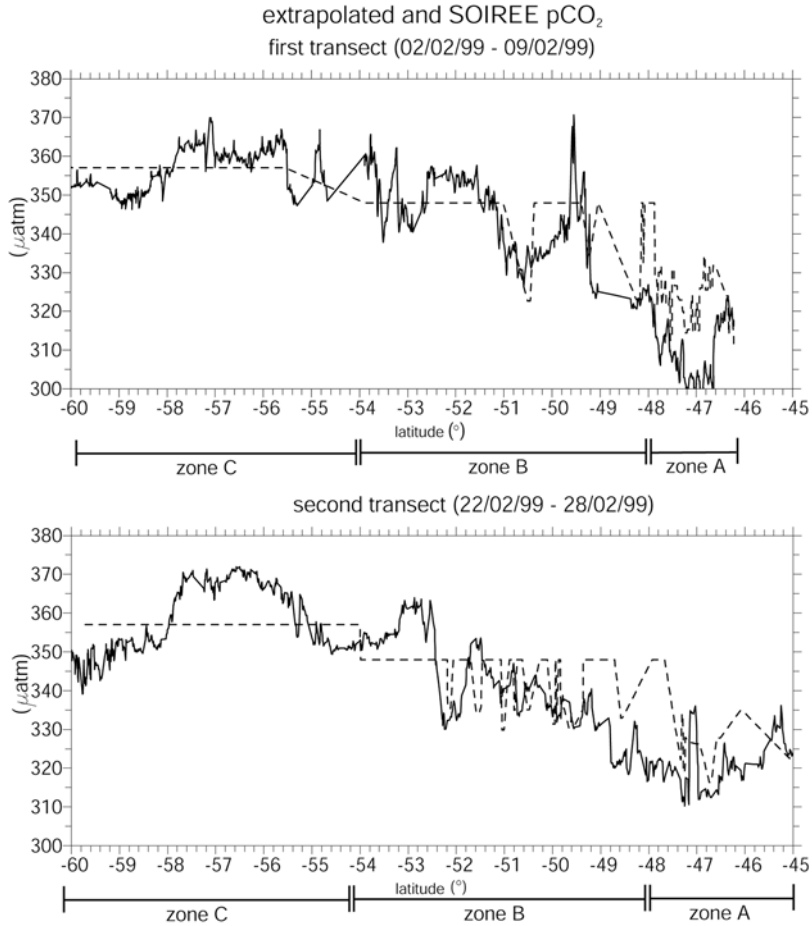

Figure 6. Variation in pCO_2 measurements (solid line) and extrapolated pCO_2 (dashed line) along SOIREE transects in February 1999 (first leg; top, second leg; bottom).

measured pCO_2 at T_{obs} becomes larger than the observed variability. This can be explained as the correction for the temperature effect does not take into account water mixing for which SST is also a tracer, thus worsening our representation of physical mechanisms and our prediction.

[30] The importance of mixing in zone B is shown by the pCO_2–SST regressions: the slope of these regressions is always negative or zero, contrary to what is expected for thermodynamical effect alone. In zone B, the mixing effect usually dominates the thermodynamical effect. It is likely that it also plays an important role in zone A.

4. Extrapolation of pCO_2

4.1. Summary of pCO_2-Chl and pCO_2-SST Fits (Standard Extrapolation Method)

[31] We keep fits between pCO_2 and SST during three periods in zone B and a yearly fit between pCO_2 and chlorophyll in zone A. The corresponding scatterplots are displayed on Figures 4a, 4b, 4c and 4e together with the fits. We also indicate the 95% confidence interval for the fits, that represents the interval in which the fit is expected to fall given the number and the scatter of the points, and the fit ± stdfit, that quantifies the scatter of the individual measurements around the fit. Figure 4d summarizes the pCO_2–SST relationships applied in the paper (including pCO_2 constant values); coefficients of the fits are reported in Table 2.

[32] Hereafter, since this method gives the best results among those tested (see below), it will be called the "standard" extrapolation method.

4.2. Quality of Extrapolated pCO_2

4.2.1. Comparison of Extrapolated pCO_2 With Independent SOIREE Measurements

[33] The drawback of the method is that it is based on a limited number of measurements and that only a few independent measurements are available for validation. We test the fits used for extrapolating pCO_2 using independent measurements from two pCO_2 SOIREE transects located between the Astrolabe and AESOPS transects. We apply the pCO_2 fits (standard scheme) using in situ SST and weekly SeaWiFS chlorophyll to compute extrapolated pCO_2 in each zone (A, B, and C) crossed by the ship's route during the Febuary 1999 SOIREE cruise. On the two transects, extrapolated and in situ pCO_2 follow the same main trends (Figure 6). South of 48°S, extrapolated pCO_2 values agree well with the measurements although, at the local-scale, differences of up to 20 µatm occur. Most of the time, differences are less than 10 µatm. North of 48°S, high-chlorophyll (zone A) are correlated with low pCO_2 values. pCO_2 drawdown in these areas is relatively well simulated (on the first leg, differences are smaller than 10 µatm). When averaged zone by zone, (see Table 3), extrapolated pCO_2 and in situ pCO_2 are very close, especially in zone B

Table 3. Comparison of Measured and Extrapolated pCO_2 Along SOIREE Transects

	Zone A			Zone B			Zone C		
	In Situ pCO_2, μatm	Predicted pCO_2, μatm	Std of Difference, μatm	In Situ pCO_2, μatm	Predicted pCO_2, atm	Std of Difference, μatm	In Situ pCO_2, μatm	Predicted pCO_2, μatm	Std of Difference, μatm
Transect 1	311	324	10.6	347	348	10.3	358	357	5.6
Transect 2	329	330	10.2	343	348	11.6	360	357	8.2

and C. The standard deviation of the difference between measured and predicted pCO_2 (6 to 12 μatm) is consistent with the precision of our regressions (2 to 9 μatm) or mean values considered in our extrapolation method in February 1999 (Table 2). This gives credibility to our extrapolation method. Even though more independent measurements at other seasons are needed for a complete validation, this result is encouraging, especially as the SOIREE transects crossed a zone where we have no measurement to develop our extrapolation method.

4.2.2. "Statistical" Error on Extrapolated pCO_2 Fields

[34] Since we do not get independent measurements at all seasons, we estimate an order of magnitude of the error on our extrapolated fields in each biogeochemical province and at seasonal scale from stdfit. Although this error estimate is not based on independent measurements, it quantifies the scatter of the measurements around the fit which is likely to be due to physical and biogeochemical processes that are not completely taken into account by the pCO_2–SST and pCO_2–chlorophyll fits.

[35] We use Reynolds SST to compute extrapolated pCO_2 maps. Then we introduce an error on pCO_2 that comes from differences between Reynolds SST and in situ SST that are used to develop pCO_2–SST fits. To quantify this error, we collocate weekly 1 × 1 degree satellite SST with SST measured during the AESOPS and Astrolabe campaigns: the mean bias is 0.03°C, and the standard deviation of the difference is 0.78°C (15 355 data points). Using the equations in Table 2, this SST uncertainty leads to an uncertainty in extrapolated pCO_2, error_from_SST, between 1.0 and 2.1 μatm.

[36] Therefore we estimate the precision of the pCO_2 extrapolated maps for zones A, B, and C as the root mean square of the quadratic sum of stdfit (Table 2) and of error_from_SST. In the following we call it statistical precision. It is always less than 8 μatm (Figure 7, top) and is smallest in fall and spring in zones B and C.

4.2.3. Alternative Extrapolation Methods Used to Determine "Methodological Error"

[37] To evaluate the sensitivity of the extrapolated pCO_2 to the biogeochemical provinces boundaries and to the variables used to fit pCO_2, we also compare results obtained with two alternative extrapolation methods derived from the same set of measurements. The difference in pCO_2 extrapolated using the standard method and the alternative methods will be referred as methodological error.

[38] In both alternative schemes, fits are derived separately for the eastern and western campaigns, assuming that the processes at play in both regions may be different, and the study area is divided at 165°W into two parts: eastern and western. This separation was not useful in the standard extrapolation method, because the chlorophyll threshold allows getting the same method valid for both transects.

[39] In the first alternative scheme (scheme I), we define province boundaries using SST thresholds (instead of Chl) and use only pCO_2-Chl fits. We define three provinces bound by north–south SST spatial gradients (larger than 1°C per 0.5° latitude) which have marked pCO_2 signatures (typically more than 10 μatm). The SST thresholds corresponding to the zones' boundaries are defined seasonally from in situ measurements, campaign by campaign, and vary from 6°C to 8°C and from 10°C to 11.5°C, respectively. In each zone, we use pCO_2–chlorophyll fits, assuming that in each zone the main effect controlling variability of pCO_2 is biological carbon uptake or water mixing and that chlorophyll is a tracer for both processes. In this scenario, we average SeaWiFS chlorophyll maps over 3 to 7 weeks centered on the corresponding cruise to minimize the number of cloudy pixels. To remove spatial variations in SeaWiFS chlorophyll that could occur at a small spatial scale, we apply a running filter over 0.5° in latitude on pCO_2 and collocated chlorophyll measurements. This scenario cannot be applied in winter because of too many cloudy pixels on SeaWiFS chlorophyll images in this season. Results obtained with this scenario are described by *Boutin et al.* [2001].

[40] The second scheme (scheme II) is very similar to the standard extrapolation method except that (1) the boundary between zones A and B is fixed (at 48°S between 140°E and 165°E and at 49°S between 165°E and 155°W), thus neglecting the variability in the spatial extent of the chlorophyll-rich zone, and (2) fits are different in the eastern and western parts.

[41] A summary of the standard deviation of the difference between pCO_2 values measured and reconstructed using each method is given in Table 4. It shows that the standard scheme better matches the measurements except in spring. This improves slightly if eastern and western campaigns are separately treated. However, this improvement may be due to the limited number of campaigns considered here. In summary we retain the standard extrapolation scheme because it allows pooling the data from the eastern and western campaigns based on biological and physical criteria, while giving similar or even lower residuals of the measurements with respect to the fits.

[42] We compare pCO_2 fields extrapolated using the standard extrapolation method with the ones obtained using alternative schemes. The maximum difference between pCO_2 fields obtained with the standard scheme and alternative schemes (Figure 7, middle) is less than 10 μatm almost everywhere in different seasons. Only in the northern part of the study area the differences between the worst performing scheme (here scheme 1) and the standard scheme are larger due to a drawback of scheme I in which low pCO_2 measurements were incorrectly interpreted as being regional instead of being caused by local high biological activity. For instance, in March the pCO_2–chlorophyll relation for the northern region of scheme I,

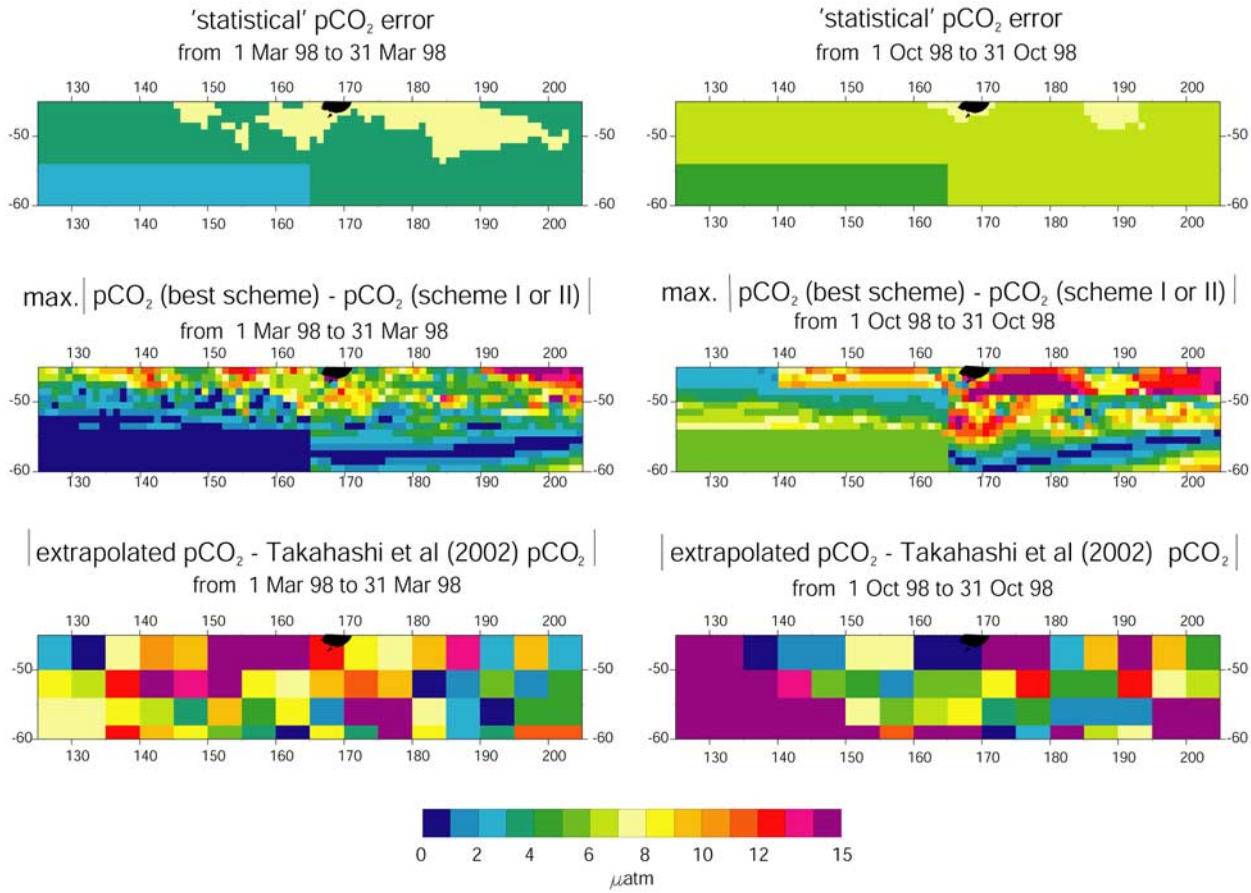

Figure 7. (top) Statistical error on pCO_2 derived with the standard scheme (see text). (middle) Maximum absolute value of the difference between pCO_2 extrapolated with the standard scheme and with one of the alternative schemes (methodological error). (bottom) Absolute difference in absolute value between extrapolated pCO_2 and *Takahashi et al.* [2002] corrected pCO_2 in March and in October 1998.

derived from AESOPS measurements made in region of high chlorophyll content, is used in regions where the chlorophyll content is low and the relation invalid.

[43] In summary, the statistical error and the methodological error are the largest in Zone A, up to 10 μatm, and minimum in zone C, up to 6 μatm; in most zones, statistical error is slightly lower than methodological error (except in zone C). The order of magnitude of statistical error and methodological error is similar to the error deduced from the comparison with SOIREE measurements.

4.3. Extrapolated pCO_2 Maps

[44] We use the standard method summarized in 4.1 to derive regional fields of ocean pCO_2 over the study area (125°E–205°E; 45°S–60°S) from December 1997 to December 1998. We choose December 1997 as the beginning of this period because summer begins in December (see definition of seasons above).

[45] Since the fits are linear, we use Reynolds SST and SeaWiFS chlorophyll data at low resolution (1 month and 1 × 1 degree) to compute monthly 1 × 1 degree extrapolated pCO_2 maps. We find a chlorophyll-rich zone (zone A) from December 1997 to April 1998 and from October 1998 to December 1998, so that from May 1998 to September 1998, the study area is composed of the zones B and C without zone A.

[46] On SeaWiFS images in December 1997 and January 1998, chlorophyll-rich areas are found in parts of the southwestern region (zone C) too. In this case, we assume that the pCO_2 decrease due to biological activity is the same as in zone A: we take a pCO_2–chlorophyll relationship with the same slope (a) as in zone A and a zero ordinate (b′) adjusted in the continuity of mean pCO_2 values in the low-chlorophyll area in zone C, $\langle pCO_2 \rangle$, as follows: the continuity is computed at ordinate (chlorophyll threshold)/2 because this is more or less the point where the fits in zone A and B join each other (except in February):

$$b' = (\langle pCO_2 \rangle \text{in zone C without chlorophyll}) - a \cdot (\text{chlorophyll threshold})/2.$$

We find b′ equal to 363 μatm in summer. Although we could not check the validity of this approach, possible errors should not have large consequences since this concerns only a few points.

[47] Monthly extrapolated pCO_2 maps for March 1998 (the beginning of fall) and for October 1998 (spring) are shown in Figure 8. In March 1998, low pCO_2 regions (less than 330 μatm) occur south of Tasmania, south and east of New Zealand. These areas are associated with chlorophyll-rich regions. In the whole study area, we find a north–south pCO_2 gradient due to negative correlation between SST and

Table 4. Standard Deviation of the Differences Between pCO_2 Measurements and Predicted Values[a] in the Whole Study Area, for Different Extrapolation Schemes

Seasons	Scheme I	Scheme II	"Standard" Scheme
Spring	6.1	4.6	5.3
Summer	10.6	11.4	9.6
Fall	6.4	5.6	4.8
Spring, summer, and fall	8.5	8.5	7.4

[a]Values are stdfit, in μatm.

pCO_2: in the northern part, pCO_2 is about 330 μatm (northeast) to 340 μatm (northwest), while in the southern part, pCO_2 is about 350 μatm (southwest) to 355 μatm (extreme southeast). Thus spatial pCO_2 variation is about 10–25 μatm from north to south and less than 10 μatm from east to west. In October 1998, pCO_2 values are higher than in March due to lower biological activity and to lower SST in October than in March. Again, low pCO_2 regions occur south and east of New Zealand, but the low pCO_2 region south of Tasmania disappears. Zone A is smaller than in March, because of lower biological activity. In the northern part, pCO_2 is relatively homogeneous (about 345 μatm) except in the chlorophyll-rich zone south and east of New Zealand. The pCO_2 value increases from north to south and is more or less homogeneous in the southern part (about 355 μatm in the southwest to 360 μatm in the southeast).

5. Monthly ΔpCO_2 and Air–Sea Fluxes Maps Deduced From Our Extrapolation and From *Takahashi* [2002] ΔpCO_2 Fields

5.1. Monthly Atmospheric pCO_2

[48] Monthly 1 × 1 degree maps of pCO_{2a} are shown in Figure 9 for March 1998 and for October 1998. We find a north–south pCO_{2a} gradient up to 10 μatm, which is stronger in March than in October. The spatial variation of pCO_{2a} is mainly due to north–south gradient of the ECMWF atmospheric pressure: in March, average Patm varies from about 1008 mbar at 45°S to 985 mbar at 60°S; in October it varies from about 1003 mbar to 986 mbar. It should be noticed that the north–south gradient of oceanic pCO_2 is positive, while the pCO_{2a} gradient is negative. Hence the north–south ΔpCO_2 gradient is enhanced by nearly 40% with respect to the gradient in oceanic pCO_2. For October, we reach to a similar conclusion. However, the north–south gradient in pCO_{2a} is weaker, about 5 μatm.

[49] Low values observed in coastal area near New Zealand are an artefact of the subsampling of ECMWF Patm maps and are due to low Patm value over New Zealand. Given the small number of rasters affected by this drawback, this does not affect significantly regionally and temporally averaged ΔpCO_2 and air–sea fluxes.

5.2. Monthly ΔpCO_2

[50] ΔpCO_2 maps are deduced as the difference between pCO_{2a} and extrapolated pCO_2 and are shown in Figure 10 (top) for March and October 1998. Because of the anti-correlation between the north–south variations of pCO_2 and pCO_{2a}, the north–south gradient of ΔpCO_2 is large (about 20 μatm). In the northern part, we observe regions with a strongly negative ΔpCO_2 between −15 and −30 μatm, because of high atmospheric pCO_2 values (about 354–358 μatm) and low oceanic pCO_2 (in the range 330–340 μatm). These areas are roughly correlated with chlorophyll-rich regions. In the southern part, oceanic pCO_2 is slightly larger than pCO_{2a}; therefore ΔpCO_2 is close to equilibrium in March and slightly positive in October.

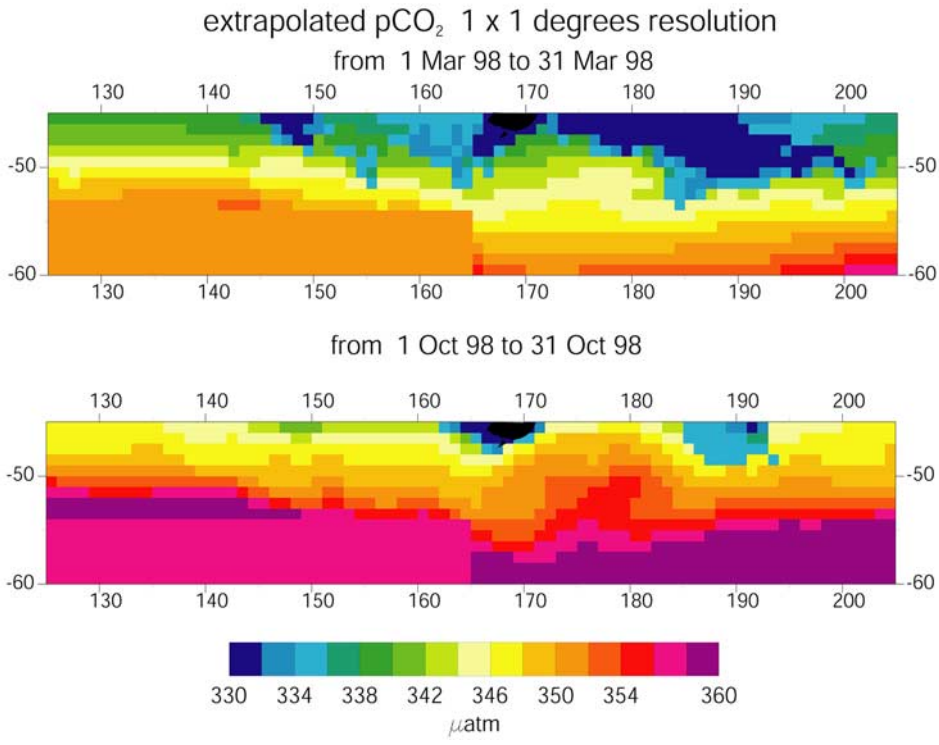

Figure 8. Extrapolated pCO_2 maps (top) in March 1998 and (bottom) in October 1998.

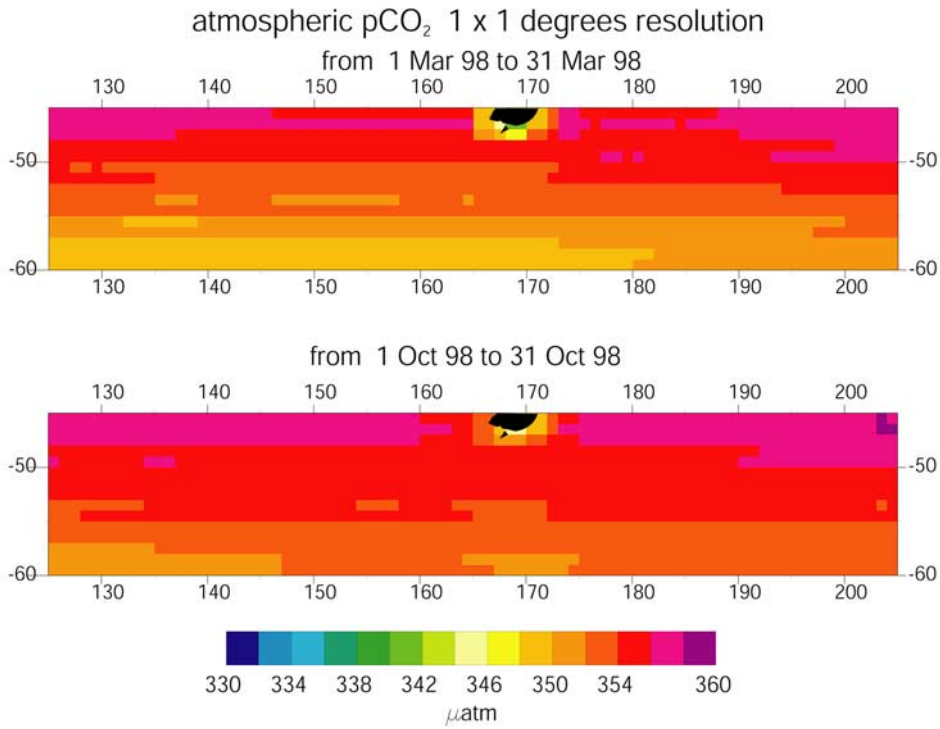

Figure 9. Atmospheric pCO_2 maps (top) in March 1998 and (bottom) in October 1998.

[51] The north–south ΔpCO_2 gradient is also seen on the climatological ΔpCO_2 maps by *Takahashi et al.* [2002] corrected for the atmospheric trend according to their assumptions (Figure 10, bottom), although the longitudinal location of the sinks is different. The spatial distribution of the absolute difference between extrapolated pCO_2 and *Takahashi et al* [2002] climatological pCO_2 is reported below statistical and methodological errors on (Figure 7, bottom). The differences with respect to Takahashi ΔpCO_2 maps are consistent with the imprecision (statistical and methodological) of our extrapolated fields in March, but not in October (pCO_2 differences up to 15 μatm). In March, the two maps exhibit the same regional patterns, in spite of local differences: on the Takahashi ΔpCO_2 map, ΔpCO_2 increases from north to south, with an absorbing region for CO_2 in the north and a slightly absorbing region in the south, whereas on our extrapolated map, ΔpCO_2 increases from absorption in the north to equilibrium to the south. On the other hand, in October, the maps disagree. Our extrapolated map shows a north–south gradient from absorption to outgassing which results in a near-zero mean air–sea flux (see below), while the Takahashi climatological map has a weak north–south gradient, with most of the study area being a sink for CO_2 and a small area close to equilibrium. In our case, the spatial variations are primarily due to north–south variations in Reynolds SST (surface water pCO_2) and in ECMWF Patm (atmospheric pCO_2). This might result from our spring pCO_2–SST regression in zone B which has a negative slope indicating a large mixing effect, whereas the Takahashi climatology was made without taking explicitly into account vertical mixing. In addition, the observed pCO_2 used to build the *Takahashi et al.* [2002] climatological pCO_2 maps vary from ±4 μatm to ±9 μatm within 4 × 5 degree pixels in the study area so that part of the discrepancy between our and Takahashi's approach may be due to small-scale (10–1000 km) variability which the two approaches treat in different ways.

[52] When analyzed over one year, the means of ΔpCO_2 are the closest in April and differ the most in October.

5.3. Monthly Net Air–Sea CO_2 Flux Maps

[53] Monthly 1 × 1 degree net air–sea CO_2 flux maps result from the product of monthly K and monthly ΔpCO_2 grids at 1 × 1 degree resolution.

[54] To examine the consequences on the air–sea flux of differences between ΔpCO_2 calculated using different grids, we compare our flux maps to monthly 1 × 1 degree air–sea CO_2 flux maps that are prepared by subsampling the 4 × 5 degree climatological mean ΔpCO_2 fields by *Takahashi et al.* [2002] and recasted onto the 1 × 1 degree ERS-2 K grids. The flux thus calculated is hereafter called the Takahashi climatological CO_2 flux. It must be noted that subgrid scale features are lost by the space-time averaging scheme used for the construction of the 4 × 5 degree field. The lost spatial information cannot be recovered by resampling the original map with a finer 1 × 1 degree resolution. Hence the Takahashi climatological maps give highly smoothed flux distributions. In addition, *Takahashi et al.* [2002] assumed that the annual mean pCO_2 in the southwestern part of the study area (125°E–180° and 50°S–60°S) did not increase with time in response to atmospheric CO_2 due to deep convective mixing, and hence applied no correction for the uptake of atmospheric CO_2. The results of a recent analysis have shown that this is not the case. Hence, in this study, we adjust the Takahashi climatology pCO_2 values from 1995 to 1997–1998 using the atmospheric increase of 1.7 uatm yr^{-1} measured at the Cape Grim station,

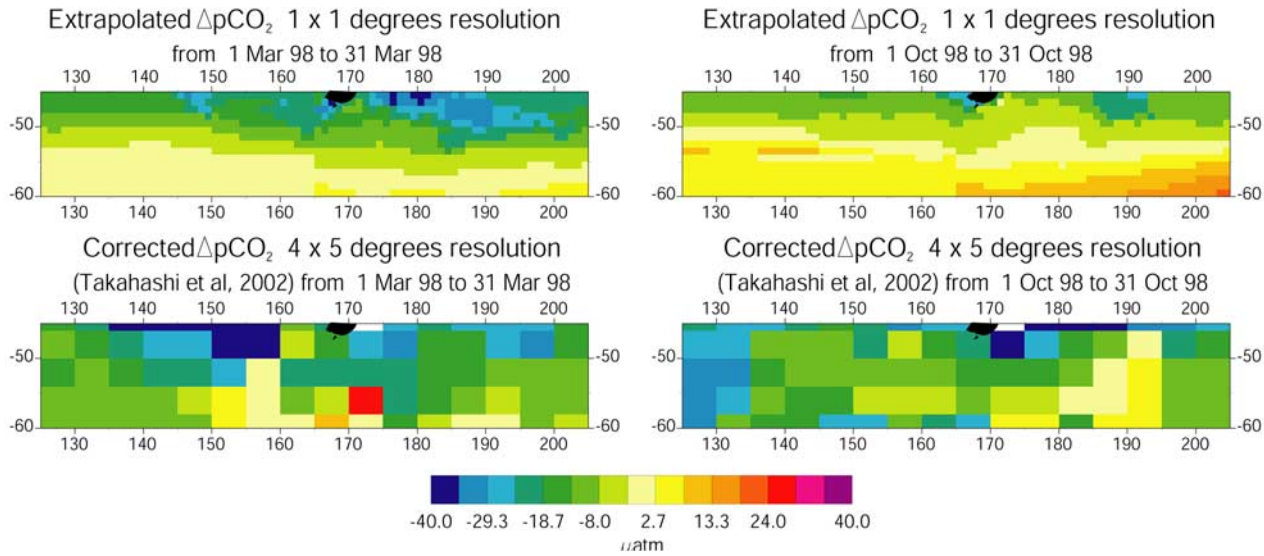

Figure 10. (top) Extrapolated ΔpCO_2 maps and (bottom) *Takahashi et al.* [2002] corrected ΔpCO_2 maps (left) in March 1998 and (right) in October 1998.

Tasmania. This assumption makes the ΔpCO_2 values in the study area less negative and thus leads to smaller ocean uptake flux values (called hereafter without correction for the atmospheric trend) as shown in Figure 12.

[55] The air–sea flux integrated over the whole area, deduced either from our extrapolation method or from the Takahashi climatological ΔpCO_2, is always toward the ocean (Figure 11).

[56] Before analyzing the differences, we need to carefully evaluate the error on each flux estimate; given that the same K were used in all flux computations, only errors on pCO_2 are considered here (uncertainties due to imprecision in K estimates are discussed in section 2.2). Assuming that there are only random errors (no systematic biases) on the Δp fields, the error on the integrated flux, Flux_error, coming from noise on Δp can be deduced from the quadratic sum of the errors in each pixel:

$$Flux\_error = \sqrt{\sum_{i=1}^{npixels} (K_i \cdot \Delta p\_error_i \cdot S_i)^2} \qquad (2)$$

where K_i, Δp_error_i and S_i are the CO_2 exchange coefficient, the error on Δp and the surface of the *i*-th pixel respectively. Concerning our extrapolation, taking the Δp_error_i in 1x1 degree pixels equal to stdfit or to std (in case no fit is used) the flux error is small and ranges between 10^{-3} GtC yr^{-1} (September) and 3 10^{-3} GtC yr^{-1} (March). Concerning the flux derived from *Takahashi et al.* [2002] pCO_2 maps, the variability of pCO_2 observations used to build the extrapolated maps in 4 × 5° pixels (4 to 9 µatm) leads to small errors on the flux as deduced from equation (2), always lower than 10^{-3} GtC yr^{-1}. However, these estimates are optimistic as systematic biases coming from imperfection in the extrapolation method are not taken into account. Hence we also consider the influence of the methodological error on our extrapolation and compare the fluxes to the ones obtained with the alternative methods. The monthly extrapolated net air–sea CO_2 fluxes determined using the 3 schemes (see section 4.2.3) (Figure 12) are very close to each other in the fall (within 0.01 GtC yr^{-1}), whereas they differ by up to 0.085 GtC yr^{-1} (peak to peak) in September and January. In the following, we will consider that the largest difference between the flux retrieved from the standard scheme (continuous line on Figure 12) and from one of the alternative scheme (dots or circles on Figure 12) is indicative of the error on the flux derived from the standard scheme. This leads to an error of 0.03 GtC yr^{-1} on the flux averaged over one year.

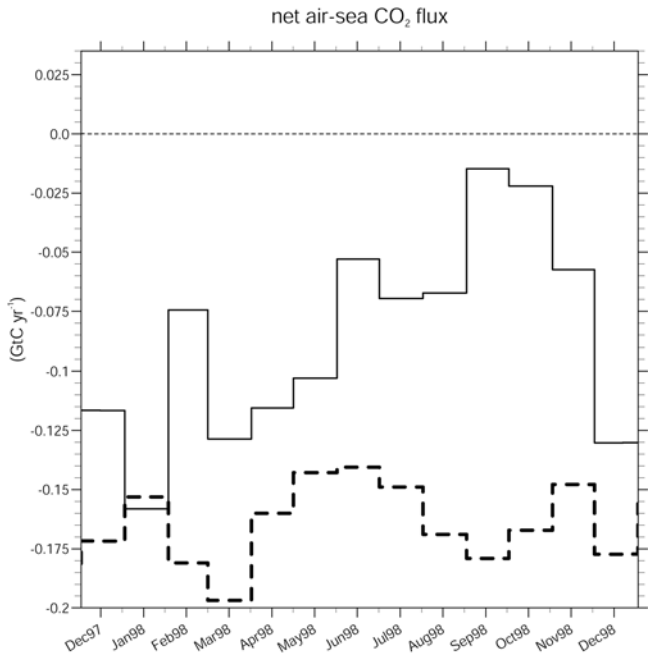

Figure 11. Extrapolated net air–sea CO_2 flux deduced from ERS-2 CO_2 exchange coefficients and pCO_2 standard extrapolation method (solid line), and *Takahashi et al.* [2002] climatological mean ΔpCO_2 fields with correction for the atmospheric trend between 1995 and 1998 (dashed line).

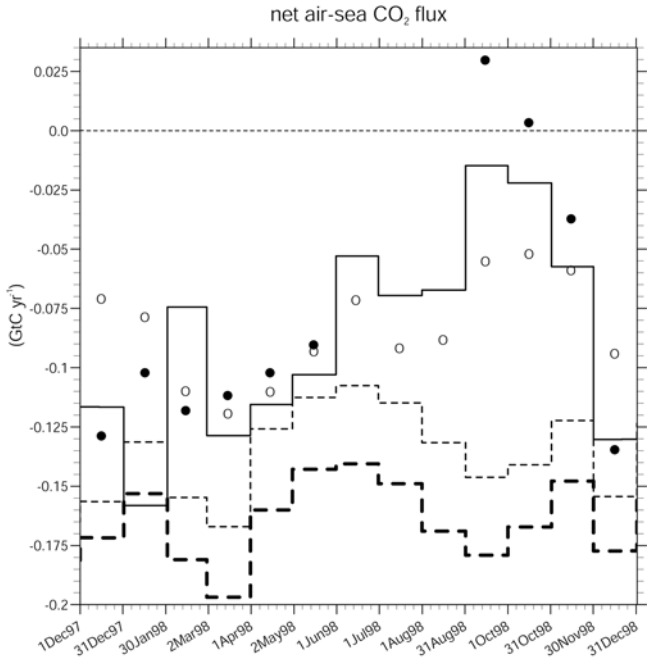

Figure 12. Extrapolated net air–sea CO_2 flux using standard extrapolation (solid line), alternative scheme I (dots) and II (open circles), (the maximum of the absolute difference between the standard extrapolation and the two alternative schemes is taken as the methodological error) and the CO_2 flux derived from the *Takahashi et al.* [2002] climatological mean ΔpCO_2 field with and without correction for the atmospheric trend (thick and thin dashed lines, respectively).

[57] Averaged over one year, the net air–sea CO_2 flux deduced from our extrapolation method is an absorption by the ocean of 0.08 GtC yr^{-1}. Its seasonal variation is large (about 0.14 GtC yr^{-1}) and overcomes the variability between December 1997 and December 1998 (the flux in December 1997 is close to the one in December 1998; the difference is about 0.015 GtC yr^{-1}). On the other hand, the Takahashi climatological flux shows a small seasonal variation (about 0.06 GtC yr^{-1}), and the minimum and the maximum of these fluxes do not occur in the same months. The Takahashi climatological CO_2 flux is maximum in winter (June 1998) and minimum in fall (March 1998), whereas our extrapolated CO_2 flux is minimum in summer (January 1998) and maximum in spring (September 1998). The Takahashi climatological CO_2 flux is always more negative than our monthly extrapolated CO_2 fluxes, except in January 1998 when it is very close (difference less than 0.02 GtC yr^{-1}). The differences are large from June 1998 to November 1998 (between 0.05 and 0.17 GtC yr^{-1}), and are maximum in September 1998 and October 1998 (about 0.15 GtC yr^{-1}). Thence *Takahashi et al.* [2002] climatological mean ΔpCO_2 fields lead to a larger absorbing flux than our extrapolation method (−0.16 GtC yr^{-1}, with correction for the atmospheric trend).

6. Discussion

[58] It is very challenging to develop an extrapolation method valid over a wide range of longitudes because processes at play may vary in longitude and the knowledge of oceanographic fronts is not sufficient to take these variations into account. For instance, *Metzl et al.* [1999] rely upon transects in two sectors in the Indian Ocean and support the idea of a different pCO_2-SST dependency in the Subantarctic Zone for each sector, with lower pCO_2 (for a given SST) in the eastern sector than in the central one. In our study one challenge is to find relationships valid both on AESOPS transects and on Astrolabe transects without degrading the precision of the fits: this is done in the Subantarctic and Polar zones (Zones A and B) in which we find relationships applicable to both transects. In addition, they are in agreement with the independent SOIREE transects.

[59] We do not extend our extrapolation method over the whole Southern Ocean, because of the lack of time series pCO_2 transects along other tracks at various seasons during the 1997–1999 period that would permit to validate them and eventually to adapt the method to other longitudes. On the other hand, using measurements made over another period would add uncertainty coming from possible interannual variability. Actually, in the Southern Ocean the oceanic trend related to the CO_2 atmospheric trend is poorly known and it may vary spatially because of the presence of upwelled waters in some part of the region: this was the assumption considered by Takahashi et al. and as we will show, such an assumption introduces large pCO_2 variations when several years are considered. Thus, before combining data measured from several years, it is essential to elucidate the interannual pCO_2 variability at the ocean surface and its relation to the atmospheric trend, a difficult exercise (given the sparcity of the data and the large spatial variability of pCO_2 related to oceanic variability), which is outside the scope of this paper. Another issue complicating the use of data from other years is the need for satellite chlorophyll. The information on chlorophyll greatly improves the extrapolation of pCO_2. To illustrate this point, we report in Table 5 the stdfit for pCO_2-SST fits in Zone A and B together. Compared to the stdfit reported in Table 2, it is clear that the use of Chl data to distinguish zones A and B reduces stdfit by a factor between 1.2 and 1.8 in zone B. In addition, pCO_2-Chl fit obtained in Zone A is of better quality than pCO_2-SST fit in Zone A, as was noticed in section 3.1.

[60] With respect to Figure 5 of *Metzl et al.* [1999] who looked at relationships of pCO_2 versus SST in the subantarctic zone of the central and eastern Indian Ocean, the slopes of our pCO_2-SST fits for Zone B are about half of their. This is because in our work pCO_2-SST fits are computed only in low Chl areas, thus excluding the very low pCO_2 values from our regressions. In their Figure 5, *Metzl et al.* [1999] study the region 45°S–46°S 13°5–155°E. From SeaWIFS Chl maps in 1997–1998, it appears that this region is 90% of the time characterized by Chl

Table 5. Statistics of pCO_2-SST Fits Obtained in Zone A and Zone B Together

Time Period	Statistics
Spring	$pCO_2 = -2.86SST + 371$ stdfit = 7.1 μatm
December	$pCO_2 = -2.53SST + 360$ Stdfit = 6.9 μatm
Fall	$pCO_2 = -4.42SST + 378$ stdfit = 4.6 μatm

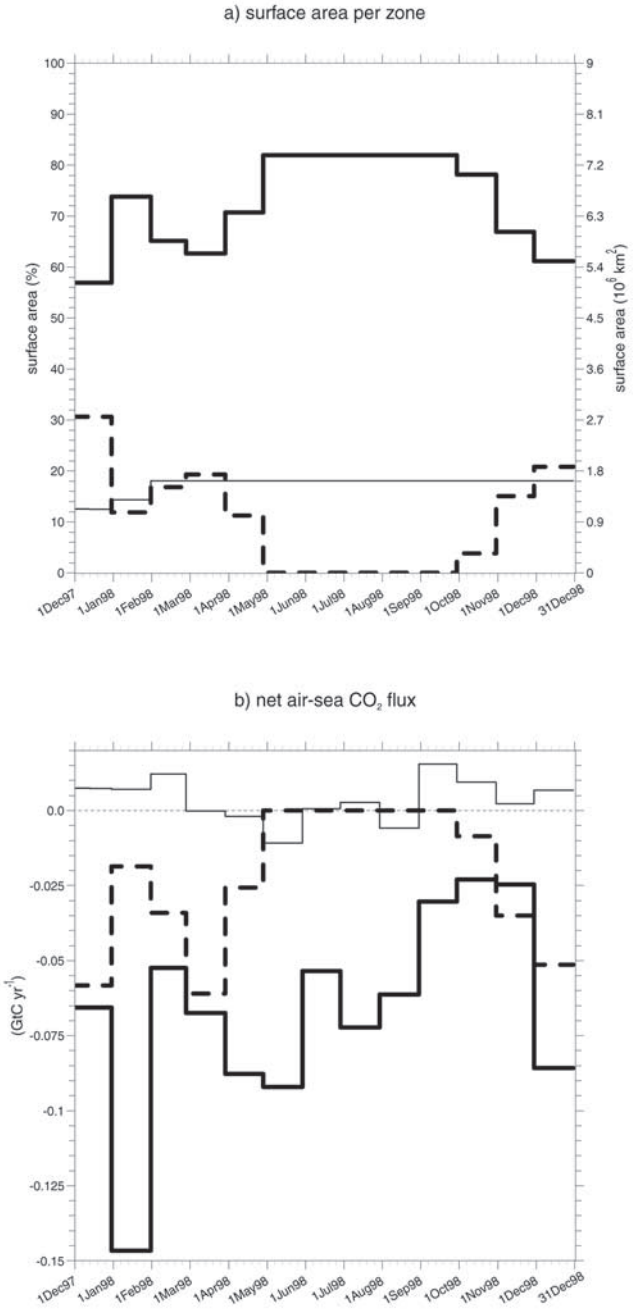

Figure 13. (a) Surface area of zone A (thick dashed line), zone B (thick solid line), and zone C (solid line) from December 1997 to November 1998. (b) Monthly extrapolated flux of CO_2 in zone A (dashed line), in zone B (thick solid line), and in zone C (solid line) from December 1997 to November 1998.

higher than 0.37 mg m^{-3}. Thus Figure 5 of *Metzl et al* [1999] has to be compared with pCO_2 versus SST in our Zone A (Figure 5). Part of the measurements we use appears to be aligned with pCO_2-SST CSIRO measurements. On the other hand, in some cases, relatively high pCO_2 values are observed together with high SST contrary to Metzl el al. study. These relatively high pCO_2 values observed both on AESOPS and Astrolabe transects are always associated with low chlorophyll values.(This is the reason why our pCO_2-Chl fits work better than pCO_2-SST fits in Zone A). These differences may be due to a change in processes driving pCO_2 variability at interannual timescale.

[61] When dealing with an extrapolation method, it is of primary importance to estimate the precision of extrapolated fields. In the present case, this is a difficult task because of the limited number of available measurements for the year 1997–1998. In addition, dividing the set of measurements into two subsets (one for developing the extrapolation, one for validating it) is not sufficient to check the validity of the extrapolation fields. The set of measurements for validation should ideally be acquired during different campaigns, at other locations and other periods than the ones used for developing the extrapolation. In this study only SOIREE transects provide independent data for validation. Thus we estimate the precision of our extrapolation method from the scatter of the pCO_2 residuals with respect to the fit (statistical approach) and from the comparison of pCO_2 extrapolated using alternative extrapolation schemes (methodological approach). The methodological error (which comes from changing the geographical locations of biogeochemical provinces, the parameter chosen as a proxy for pCO_2 variation [SST or chlorophyll], etc.) is in most places larger than the statistical error and is likely to be an upper bound to the true methodological error since the standard scheme was chosen to minimize the residuals of the measurements to the fits, while having the most general approach and being based on a representation of physical and biological phenomena. Nevertheless, the methodological errors are compatible with errors deduced from SOIREE measurements in summer in Zone A and B. In the absence of independent measurements in all zones and in all seasons, we take them as indicative to deduce errors on the air–sea flux. From SOIREE comparisons, it seems that methodological errors in Zone C are underestimated but this has a weak impact on the flux error estimate as the flux is weak in Zone C. In winter, we have no data and extrapolation method is derive as a mean of spring and fall measurements so that error in winter may be underestimated.

[62] Extrapolated ΔpCO_2 are less negative than *Takahashi et al.* [2002] climatological ΔpCO_2 except in small areas (Figure 10). These ΔpCO_2 differences lead to significant differences in the air–sea CO_2 fluxes. Seasonal variation obtained with our extrapolated pCO_2 is larger, although, in the Takahashi climatology maps, space-time variability was smoothed by averaging over the 30 years of time and 4 × 5 degree pixel size. The Takahashi CO_2-corrected fluxes are always more negative than our extrapolated CO_2 flux, as Figure 11 shows. These differences cannot be explained by errors we estimate on our extrapolation method using our methodological approach. Therefore we look at errors linked to the assumptions on interannual variability. We consider the monthly Takahashi climatological CO_2 flux derived either from ΔpCO_2 corrected for the atmospheric trend of 1.7 μatm yr^{-1} between 1995 and 1997–1998, as described in section 5.3, or computed for a reference year (1995). The correction for the atmospheric trend makes the absorbed flux to increase by 0.015 to 0.035 GtC yr^{-1} (depending on the month) with respect to the flux deduced from the 1995 ΔpCO_2 fields. We find that the Takahashi climatological CO_2 flux matches better

our estimates when no correction for the atmospheric trend is applied and that the differences between the two flux estimates cannot be explained by the methodological error in February and March and from June to November. Although the correction for the atmospheric trend is not applied over the whole study area, it is responsible for a decrease in the yearly CO_2 sink of 0.03 GtC yr^{-1} (from -0.13 GtC yr^{-1} to -0.16 GtC yr^{-1}, without and with correction for the atmospheric trend, respectively). This stresses the importance of knowing accurately how the surface ocean pCO_2 is affected by the atmospheric trend.

[63] Part of the disagreement between our and *Takahashi et al.* [2002] pCO_2 estimates may come from the conceptual differences between the two approaches. We use few campaigns (eight north–south transects) and a regression approach to extrapolate pCO_2 measurements over the study area. Thus this analysis is mainly driven by spatial variability (only eight periods of time) and excludes interannual variations. In contrast to this approach, *Takahashi et al.* [2002] computed their global climatological mean estimates using a longest pCO_2 database with campaigns conducted between 1958 and 2000, thus making assumptions on interannual variability, in a larger region and using a lateral two-dimensional advection–diffusion transport equation to extrapolate these measurements.

[64] From the net air–sea CO_2 flux in zone A, B, and C, we observe that most of the areas with strong CO_2 uptake are linked with chlorophyll-rich areas. It is therefore important to know the CO_2 flux in these areas and whether this flux represents a large part of the total flux in the study area. Hence we look at the mean value of our extrapolated flux of CO_2 in each zone (A, B, and C) separately. The surface area of these zones changes each month (see Figure 13a). Zone B represents 60% to 80% of S (S is defined as the total area of the study area and is equal to about 9.10^6 km^2), zone C represents 15% to 20% of S and zone A represents up to 30% of S. Zone A exists only from December 1997 to May 1998 and from October 1998 to December 1998. Our monthly CO_2 flux estimate for each zone is shown in Figure 13b. From January 1998 to December 1998, we find a CO_2 sink equal to $-6.6.10^{-2}$ GtC yr^{-1} in zone B, -2.10^{-2} GtC yr^{-1} in A and $0.35.10^{-2}$ GtC yr^{-1} in C. The mean flux of CO_2 in zone B represents about 80% of the total flux because it is associated with the largest area. The CO_2 flux in zone C is always very small (close to equilibrium). The absolute CO_2 flux in zone A is more than the CO_2 flux in C although A and C have a comparable surface area. In addition, we find that the CO_2 sink in zone A represents about 24% of the total sink. Therefore, at the annual scale, most of the flux is absorbed in zone B. Nevertheless, the monthly flux in zone A is close to monthly flux in zone B during several months (December 1997, March 1998, and November 1998) and is responsible for most of the seasonal variation of the net air–sea flux over the whole area.

7. Conclusion

[65] We analyze in situ measurements and we develop a method for estimating net air–sea CO_2 fluxes south of Australia and New Zealand (22% of the area of the Southern Ocean between 45°S and 60°S) using remotely sensed measurements. We predict the spatial distribution and temporal variation of the fluxes from satellite data and are able to determine the origin of this variation. We show that the oceanic pCO_2 distribution is mostly controlled by biological activity in regions where the chlorophyll concentration is above a given threshold,, whereas it appears to be primarily driven by water mixing in other parts of the subantarctic and polar zones,. However, the effect of biological activity in these low-chlorophyll regions probably also plays a role in depleting the region in CO_2 and is implicitly taken into account.

[66] We also show that the north–south gradient of atmospheric pressure leads to significant ΔpCO_2 variation.

[67] The study area is always a sink for atmospheric CO_2. The absorbed flux of CO_2 amounts to -0.08 GtC yr^{-1}, which is less than the absorption flux computed from *Takahashi et al.* [2002] climatological pCO_2 maps by a factor of 1.6 to 2, depending on whether or not a correction is applied for the atmospheric trend. This strengthens the need for accurately assessing how pCO_2 at the ocean surface follows or not the pCO_2 increase in the atmosphere. In summer and fall, the fluxes obtained by the two approaches are close. The differences observed in spring and in winter are not easily explained since there are no in situ measurements available: the observed differences depend uniquely on the extrapolation methods used in both approaches. It is therefore essential to gather in situ measurements during these seasons. In order to spatially and temporally extend this kind of extrapolation method confidently, interannual variability of oceanic pCO_2 needs to be addressed such that measurements from several years intervals may be combined. This requires long-term monitoring of pCO_2 in the Southern Ocean.

Appendix A: Computation of pCO_2 From CO_2 Concentration Measurements

[68] In each campaign, sea surface pCO_2 is deduced from in situ measurements of the CO_2 concentration in dry air, xCO_2 in an equilibrator. The CO_2 partial pressure in the equilibrator, pCO_{2eq} is estimated as

$$pCO_{2eq} = xCO_2 \cdot [Peq - pH_2O] \quad (A1)$$

where Peq is the total pressure under which the gas and seawater were equilibrated and pH_2O is the saturated water pressure at equilibrator temperature. pH_2O is derived from the temperature in the equilibrator and from the formulation of *Weiss and Price* [1980]. Then, surface pCO_2 is derived from pCO_{2eq}, by correcting it for the difference between in situ and equilibrator temperature using a temperature effect of $0.0423°C^{-1}$. In the case of the Astrolabe campaigns, Peq was not measured. However, it is expected to be close to the atmospheric pressure (Patm). Patm was also not measured on these campaigns, so ocean pCO_2 has been derived from xCO_2 using Patm inferred from the ECMWF atmospheric model (ECMWF Patm) at high resolution (temporal resolution: 6 hours, spatial resolution: 1×1 degree). It should be noticed that in the Southern Ocean, Patm can be very low: on average over the two campaigns, Patm is 1000 mbar and can be as low as 971 mbar (minimum for these campaigns). Hence, when dealing with measurements

made at a pressure close to the atmospheric pressure, one must pay great attention to Peq: an error of 40 mbar in Peq induces an error of 4% in pCO_2 (about 14 μatm).

[69] **Acknowledgments.** We are very much indebted to Cathy Boonne for providing the atmospheric pressure data inferred from the ECMWF atmospheric model and Olivier Coze, Nicolas Martin and Stephanie Contardo for processing support. CERSAT/IFREMER produced the level 2 ERS-2 wind speed data. The SeaWiFS project and DAAC/GSFC produced and distributed the SeaWiFS data. We note sadly that this is a posthumous contribution from our colleague, Michel Frankignoulle, who passed away in March 2005. This study was supported by the following French national programs: CNES/TAOB and CNRS-PROOF/FLAMENCO2.

References

Bakker, D. C. E., A. J. Watson, and C. S. Law (2001), Southern Ocean iron enrichment promotes inorganic carbon drawdown, *Deep Sea Res., Part II*, *48*, 2483–2507.

Belkin, I. M., and A. L. Gordon (1996), Southern Ocean fronts from the Greenwich meridian to Tasmania, *J. Geophys. Res.*, *101*, 3675–3694.

Boutin, J., Y. Rangama, J. Etcheto, L. Merlivat, T. Takahashi, B. Delille, and M. Frankignoulle (2001), Variability of the air–sea CO_2 fluxes inferred from in situ and remotely sensed parameters in the Southern Ocean, paper presented at the Sixth International Carbon Dioxide Conference, World Meteorol. Org., Sendai, Jpn.

Boutin, J., J. Etcheto, L. Merlivat, and Y. Rangama (2002), Influence of gas exchange coefficient parameterisation on seasonal and regional variability of CO_2 air–sea fluxes, *Geophys. Res. Lett.*, *29*(8), 1182, doi:10.1029/2001GL013872.

Frankignoulle, M., A. Borges, and R. Biondo (2001), A new design of equilibrator to monitor carbon dioxide in highly dynamic and turbid environments, *Water Resour. Res.*, *35*(5), 1344–1347.

Frew, N. M., E. J. Bock, U. Schimpf, T. Hara, H. Haussecker, J. B. Edson, W. R. McGillis, R. K. Nelson, S. P. McKenna, M. B. M. Uz, and B. Jahne (2004), Air–sea gas transfer: Its dependence on wind stress, small-scale roughness and surface films, *J. Geophys. Res.*, *109*, C08S17, doi:10.1029/2003JC002131.

GlobalView–CO_2 (2003), Cooperative Atmospheric Data Integration Project–Carbon Dioxide [CD-ROM], Climate Monit. and Diagn. Lab., Natl. Oceanic and Atmos. Admin., Boulder, Colo.

Gloor, M., N. Gruber, J. Sarmiento, C. L. Sabine, R. A. Feely, and C. Rödenbeck (2003), A first estimate of present and preindustrial air–sea CO_2 flux patterns based on ocean interior carbon measurements and models, *Geophys. Res. Lett.*, *30*(1), 1010, doi:10.1029/2002GL015594.

Gurney, K. R., et al. (2004), Transcom 3 inversion intercomparison: Model mean results for estimation of seasonal carbon sources and sinks, *Global Biogeochem. Cycles*, *18*, GB1010, doi:10.1029/2003GB002111.

Liss, P. S., and L. Merlivat (1986), Air–sea gas exchange rates: Introduction and synthesis, in *The Role of Air–Sea Exchange in Geochemical Cycling*, edited by P. Buat-Ménart, pp. 113–127, Springer, New York.

Metzl, N., B. Tilbrook, and A. Poisson (1999), The annual fCO_2 cycle and the air–sea CO_2 flux in the sub-Antarctic ocean, *Tellus, Ser. B*, *51*, 849–861.

Moore, J. K., and M. R. Abbott (2000), Phytoplankton chlorophyll distributions and primary production in the Southern Ocean, *J. Geophys. Res.*, *105*, 28,709–28,722.

Morrison, J. M., S. Gaurin, L. A. Codispoti, T. Takahashi, F. J. Millero, W. D. Gardner, and M. J. Richardson (2001), Seasonal evolution of hydrographic properties in the Antarctic Circumpolar Current at 170°W during 1997–1998, *Deep Sea Res., Part II*, *48*, 3943–3972.

Nightingale, P. D., G. Malin, C. S. Law, A. J. Watson, P. S. Liss, M. I. Liddicoat, J. Boutin, and R. C. Upstill-Goddard (2000), In-situ evaluation of air–sea gas exchange parameterisations using novel conservative and volatile tracers, *Global Biogeochem. Cycles*, *14*, 373–387.

Orsi, A. H., T. Whitworth III, and W. D. Nowlin Jr. (1995), On the meridional extent and fronts of the Antarctic Circumpolar Current, *Deep Sea Res., Part I*, *42*, 641–673.

Peacock, S. (2004), Debate over the ocean bomb radiocarbon sink: Closing the gap, *Global Biogeochem. Cycles*, *18*, GB2022, doi:10.1029/2003GB002211.

Reynolds, R. W., and T. M. Smith (1994), Improved global sea surface temperature analyses using interpolation, *J. Clim.*, *7*, 929–948.

Rubin, S. I. (2003), Carbon and nutrient cycling in the upper water column across the Polar Frontal Zone and Antarctic Circumpolar Current along 170°W, *Global Biogeochem. Cycles*, *17*(3), 1087, doi:10.1029/2002GB001900.

Sweeney, C., E. M. Gloor, J. A. Jackobson, R. M. Key, G. McKinley, and J. L. Sarmiento (2004), Estimating air-sea gas exchange using bomb ^{14}C: Revisited, paper presented at SOLAS Science 2004, Surface Ocean–Lower Atmos. Study, Halifax, Nova Scotia, Canada.

Takahashi, T., C. Sweeney, S. C. Sutherland, D. W. Chipman, J. Goddard, and S. I. Rubin (2000), Method of underway pCO_2 measurements in surface waters and the atmosphere during the AESOPS Expeditions, 1996–1998 in the Pacific sector of the Southern Ocean and the Ross Sea, U.S. JGOFS Data Cent., Woods Hole Oceanogr. Inst., Woods Hole, Mass.

Takahashi, T., et al. (2002), Global sea–air CO_2 fluxes based on climatological surface ocean pCO_2 and seasonal biological and temperature effects, *Deep Sea Res., Part II*, 1601–1622.

Wanninkhof, R. (1992), Relationship between wind speed and gas exchange over the ocean, *J. Geophys. Res.*, *97*, 7373–7382.

Wanninkhof, R., and W. R. McGillis (1999), A cubic relationship between air–sea CO_2 exchange coefficient and wind speed, *Geophys. Res. Lett.*, *26*, 1889–1892.

Wanninkhof, R., K. F. Sullivan, and Z. Top (2004), Air–sea gas transfer in the Southern Ocean, *J. Geophys. Res.*, *109*, C08S19, doi:10.1029/2003JC001767.

Watson, A. J., D. C. E. Bakker, P. W. Boyd, A. J. Ridgwell, and C. S. Law (2000), Effect of iron supply on Southern Ocean CO_2 uptake and implications for glacial atmospheric CO_2, *Nature*, *407*, 730–733.

Weiss, R. F., and B. A. Price (1980), Nitrous oxide solubility in water and seawater, *Mar. Chem.*, *8*, 347–359.

D. C. E. Bakker, School of Environmental Sciences, University of East Anglia, Norwich NR4 7TJ, UK.

J. Boutin, J. Etcheto, L. Merlivat, and Y. Rangama, Laboratoire d'Océanographie Dynamique et de Climatologie/Institut Pierre Simon Laplace, Université Pierre et Marie Curie, 4 Place Jussieu, 75252 Paris, France. (jb@lodyc.jussieu.fr)

B. Delille, Unité d'Océanographie Chimique, Université de Liège, Allée du 6 Août, 17 4000 Liège, Belgium.

T. Takahashi, Lamont-Doherty Earth Observatory of Columbia University, Palisades, NY 10964, USA.